Electrical characteristics of low temperature densified barium titanate

Levent Karacasulu[a], Melike Tokkan[a], Mauro Bortolotti[b], Gloria Ischia[b], Umut Adem[a], Cekdar Vakifahmetoglu[a,*]

[a] *Department of Materials Science and Engineering, Izmir Institute of Technology, 35430, Urla, Izmir, Turkey*
[b] *Department of Industrial Engineering, University of Trento, Via Sommarive 9, 38123, Trento, Italy*

ABSTRACT

A low temperature densification technique, i.e. reactive hydrothermal liquid-phase densification (rHLPD) was followed to obtain highly dense $BaTiO_3$ components at temperatures $\leq$ 240 °C. The formed ceramics were characterized concerning not only the structural features but also the electrical properties. The increase of both reaction time and temperature resulted in enhanced densification of $BaTiO_3$ components reaching about 90% of theoretical density. The presence of the tetragonal $BaTiO_3$ was demonstrated by both XRD and TEM analysis. Despite the low reaction temperatures, the samples showed promising dielectric, ferroelectric and piezoelectric functionality without additional annealing. A broad dielectric peak was observed around 135 °C at the Curie temperature; saturated hysteresis loops and corresponding butterfly-shaped strain-electric field loops were obtained. $BaTiO_3$ sample subjected to hydrothermal reaction at 240 °C for 72 h yielded a piezoelectric coefficient of 84 pC/N.

1. Introduction

Generally speaking, ceramic components are processed at high temperatures by following traditional sintering methods namely solid state, liquid phase, pressure-assisted sintering, etc. Recently, different sintering approaches that allow the densification of ceramic artifacts at temperatures below around 400 °C, i.e. low temperature densification techniques which are broadly called as cold sintering (CS), have been proposed [1]. Among others, rHLPD process is a concept of low temperature densification consisting of an infiltration, hydrothermal reaction, and reactive crystallization. Firstly, conventional shaping techniques are used to form a porous matrix. Then, the structure is infiltrated with a solution including reactive species, followed by hydrothermal reaction, similar to ordinary crystallization studies [2]. However, specifically for rHLPD during the hydrothermal process; the pores act as local micro-reactors and depending on the molar volume expansion of the aimed reaction, theoretically, 100% dense components can be obtained. In other words; the only requirement of the process is a hydrothermal crystallization reaction with reaction products having a higher molar volume compared to that of the green body [3].

Barium titanate ($BaTiO_3$) is one of the most well-known ferroelectric materials. It is widely used in electrical applications such as multilayer capacitors due to its high dielectric constant and low dielectric losses [4,5]. While highly dense $BaTiO_3$ components were produced by high

temperature sintering via various processes such as two step sintering [6,7], hot isostatic pressing [8,9], spark plasma sintering [4,10–12], and flash sintering [13,14], relatively limited number of works were published concerning the low temperature densification of $BaTiO_3$ [3,15–20]. Guo et al. [16,17] utilized a $BaTiO_3$ powder having bimodal particle size distribution. Water assisted powder was subjected to a CS process at 180 °C for 3 h resulting in a high densification reaching to 94.4%. However, the samples produced by CS showed limited dielectric properties, i.e. no peak appeared in the dielectric constant at the Curie temperature and dielectric constant remained quite low up to 200 °C. Because of such an issue, an additional annealing process (at 900 °C for 3 h) was conducted and the dielectric properties were improved. In another study, a $BaTiO_3$ powder (< 100 nm particle size) was used for CS under similar conditions, resulting in the samples with relative density above 96% yet comparable additional heat treatment at 900 °C was followed to enhance the dielectric properties [18]. While in those works $BaTiO_3$ was formed by following CS, rHLPD was also followed to produce $BaTiO_3$ starting from a TiO_2 pellet and $Ba(OH)_2$ solution under hydrothermal conditions [3]. Although the process kinetics, densification and mechanical properties of the samples were analyzed, the electrical properties of such components were never discussed. Therefore, in this study, it was aimed to investigate dielectric, ferroelectric and piezoelectric properties of the $BaTiO_3$ ceramics densified via rHLPD at temperatures below 240 °C.

2. Experimental procedure

3 g of Titanium oxide (TiO_2, titania) (Anatase, 99.8%, Sigma Aldrich, CAS#: 1317-70-0) powder was mixed in 12 ml of deionized (DI) water with a gram of 10 wt% polyvinyl alcohol (PVA) aqueous solution for 24 h using a planetary ball mill (Retsch PM-100, Germany) in a high density polyethylene (HDPE) jar with zirconia balls. The TiO_2 suspension was then dried, sieved, and pressed uniaxially at 30 MPa into 10 mm-disc-shaped pellets. The green samples were heated to 400 °C for PVA binder burnout procedure.

Barium hydroxide ($Ba(OH)_2.8H_2O$) (> %98, Acros Organics, CAS#: 12230-71-6) was used as barium source. The pressed pellets were first subjected to pre-infiltration by wetting the sides of the green-body with a prepared solution of barium hydroxide, followed by placement of the sample into the Teflon liner containing vessel (Parr Instruments 4748 model, USA), addition of the reaction solution, hydrothermal processing at 180 °C and 240 °C up to 72 h, washing by DI water and drying. The obtained samples were coded as BT1 for the sample formed at 240 °C for 24 h, and BT2 for the one obtained at 240 °C for 72 h. Similarly the samples produced at 180 °C for 24 h and 72 h were coded as BT3 and BT4, respectively.

The bulk densities were measured by Archimedes' method. The data together with the calculated theoretical density from rule of mixtures (ROM by taking the Rietveld volume fractions) value were used to find out the final relative densities. X-ray diffraction measurements were performed on a Rigaku D-Max III (Tokyo, Japan) instrument operating in Bragg-Brentano geometry and equipped with a Copper anode X-Ray source ($Cu_{k\alpha}$ = 1.5406 Å at 40 kV, 30 mA), diffracted beam graphite monochromator, 1° divergence and receiving slit and 5° diffracted beam Soller slits. Scans were performed over the 5°–135° (2Θ) range, with a 0.02° step size and 2 s counting time per step. Instrumental broadening was characterized by means of an Y_2O_3 powder (99.99%, Sigma-Aldrich, CAS#: 1314-36-9) annealed at 1400 °C for 24 h. The morphological properties and microstructure were analyzed by using a scanning electron microscope (SEM, FEI, Quanta 250 FEG, USA) and a transmission electron microscopy (TEM, ThermoFisher Talos F200S FEG, Netherlands) operating at 200 kV. Prior to SEM analysis all the samples were coated by sputter coating. TEM sample was prepared suspending a small amount of powder in ethanol, performing a 5 min sonication treatment and putting 50 μL of solution on a TEM copper grid covered by amorphous carbon.

In order to measure the electrical properties, silver epoxy was deposited on the surface of the pellets to form electrical contacts. The silver epoxy was cured at 135 °C for 7 min. Dielectric properties were evaluated using a Keysight E4980AL Precision LCR meter (USA) between room temperature (RT) and 250 °C. Ferroelectric hysteresis loop measurements were done using an Aixacct TF Analyzer 1000 (Germany) at RT. To assess the piezoelectric coefficient d_{33}, a d_{33} meter (Sinocera Piezoelectronics, YE2730A, China) was used. Poling of the samples was carried out at 70 °C for 15 min under electric fields larger than 35 kV/cm [21], also using the Aixacct instrument.

3. Results & discussion

The relative density (RD) of green TiO_2 pellets prepared by dry pressing was about 0.55. After rHLPS process, the obtained final densities of $BaTiO_3$ samples are given in Table 1. As expected, the relative density of the final components was enhanced with increasing reaction time and temperature. The sample coded as BT2 which was subjected to rHLPS at 240 °C for 72 h demonstrated the highest relative density reaching 86.8%, resembling the previous studies [3]. The XRD plots obtained from whole set of samples are given in Fig. 1, exhibiting clearly similar diffraction features between each other; reference reflection marks for tetragonal $BaTiO_3$ (ICDD PDF# 00-005-0626) are also reported on the bottom of the plot, and the occurrence of other peaks belonging to residual TiO_2 is visible.

Table 1
The relative densities, quantitative parameters obtained from Rietveld refinements, Curie temperature (T_c), remanent polarization (P_r), coercive field (E_c) and maximum polarization (P_m) values of all samples.

| Sample	BT1	BT2	BT3	BT4
T (°C)	240	240	180	180
t (h)	24	72	24	72
RD (*100)	80.1	86.8	71.3	74.3
Goodness of Fit	2.89	3.02	3.06	2.92
$BaTiO_3$ (vol %)	89.24	95.40	85.03	88.31
TiO_2 (vol %)	9.47	3.80	14.06	10.46
$BaCO_3$ (vol %)	1.29	0.79	0.91	1.23
$BaTiO_3$ crystal size (Å)	392	494	461	464
$BaTiO_3$ cell a (Å)	4.0041	4.0024	4.0088	4.0081
$BaTiO_3$ cell c (Å)	4.0255	4.0257	4.0252	4.0246
$BaTiO_3$ c/a ratio	1.0053	1.0058	1.0041	1.0041
$BaTiO_3$ cell volume (Å3)	64.530	64.485	64.686	64.656
T_C (°C) at 10 kHz	140	135	142	142
P_r (μC/cm²)	2.10	1.72	1.22	1.40
E_c (kV/cm)	8.1	5.52	8.5	6.82
P_m (μC/cm²)	6.03	7.44	4.39	5.68
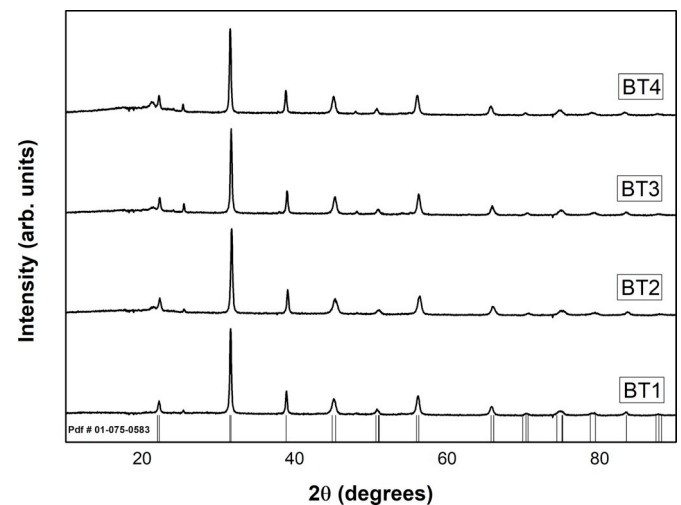
Fig. 1. The normalized XRD patterns obtained from the whole set of samples. At the bottom of the experimental data, reference reflection marks for tetragonal $BaTiO_3$ (ICDD PDF# 00-005-0626) are given.

Quantitative powder diffraction analysis was performed by full-profile Rietveld approach as implemented in the software ReX [22], by starting from a three-phase mixture model ($BaTiO_3$ [23], TiO_2 [24] and $BaCO_3$ [25]) and refining the volume fractions of all the phases as well as the lattice parameters and average volume-weighted crystallite size of $BaTiO_3$ [26]. For the refinement, both cubic and tetragonal symmetries of $BaTiO_3$ were tested; the best fit was obtained by using the tetragonal phase, whose presence was also confirmed in a conclusive manner by TEM observation (see later). Despite the absence of an evident tetragonal peak splitting in the XRD patterns, a larger peak broadening can be observed in corresponding reflections (e.g. (2 0 0)), which is indeed better accounted for by modeling the data with the tetragonal phase and independently fitting the a and c cell parameters. As an example, the refinement plot obtained from BT2 sample is shown in Fig. 2 (for all sample sets, the refined quantitative values are given in Table 1.). Both the flatness of the residual error curve and the goodness of fit, R (%) values ranging from 2.89 to 3.06, indicate an accurate modeling of the diffraction data. It could be seen that the amount of TiO_2 decreases with increasing processing time. In a similar fashion; when the reaction temperature was increased from 180 °C to 240 °C, titania amount was reduced considerably. Similar to other studies, $BaCO_3$ was also detected but was always below 1.5 vol%, this is as
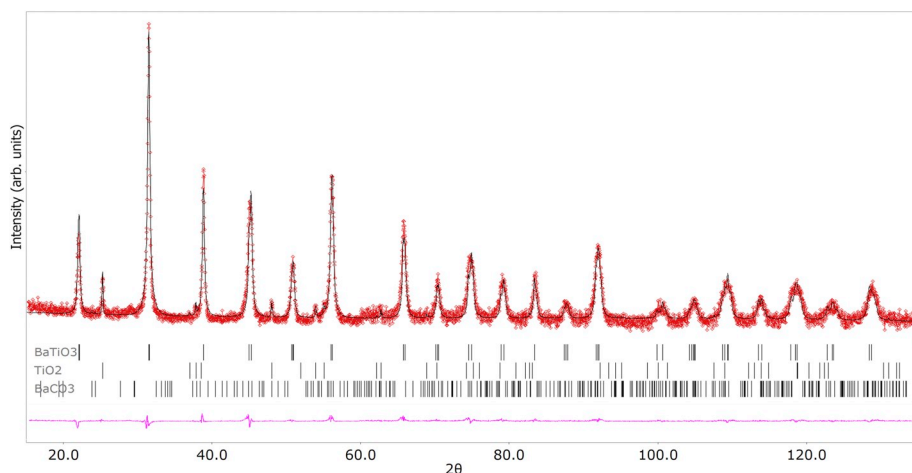
Fig. 2. Rietveld refinement of the x-ray diffraction pattern (the straight black lines correspond to the experimental data, the red dots correspond to the calculated pattern, and below the pattern, first the peak positions for BaTiO₃, TiO₂ and BaCO₃ and then the residual fitting error plot is given), for the sample reacted for 72 h at 240 °C. (For interpretation of the references to colour in this figure legend, the reader is referred to the Web version of this article.)

known to be a common problem when $BaTiO_3$ was synthesized under hydrothermal reaction conditions from $Ba(OH)_2$ and TiO_2 [3,27–29].

The tetragonality of the $BaTiO_3$ phase was followed starting from the reference phase [3] and refining both the a and c parameters in the analysis. Reaction temperature seems to have the greatest effect on the c/a ratio, followed by reaction time. Accordingly, sample BT2 exhibits the highest c/a value (1.0058), followed by sample BT1 (1.0053); samples processed at lower temperature (180 °C), i.e. BT3 and BT4 presented the lower value (1.0041) with no significant differences. The c lattice parameter remains relatively stable among the different samples whereas parameter a decreases when both the reaction time and temperature increases, implying the enhancement in the tetragonality; similarly as indicated in the previous studies that systems subject to longer reaction times or higher temperatures resulted in higher tetragonality [30]. As a consequence, $BaTiO_3$ cell volume follows the same trend, with BT2 showing the lowest volume and BT3 being the highest, and BT1 and BT4 exhibiting intermediate values. On the other hand, average volume-weighted crystallite size did not show any clear dependence on reaction time and/or temperature, with the exception of BT2 sample showing the highest value; it has to be noted that crystallite size, being defined as the average volume of coherently scattering crystalline domains, differs in general from grain size (as observed e.g. from SEM images, see later), and the two are thus not simply comparable.

SEM image taken from the fracture surface of the un-reacted TiO_2 pellet, i.e. the starting green substrate body is shown in Fig. 3(a). While from the fracture surface of the green body, porosity and some agglomeration can be seen, the sample subjected to hydrothermal reaction at 240 °C for 72 h demonstrated to have a relatively dense structure, see Fig. 3(b), corroborating the data given in Table 1.

TEM images obtained from the densest sample (BT2) are given in Fig. 4(a&b). No core/shell structure was found in the analyzed particles. The particles have dimensions ranging from few hundred nanometers to

microns. The same sample was also investigated through selected area electron diffraction (SAED); the obtained diffraction pattern was indexed by using the ProcessDiffraction software [31]. The spectrum was compared with the $BaTiO_3$ tetragonal card, see Fig. 4(c). The presence of the tetragonal $BaTiO_3$ structure is consistent with the doubling of the peaks evident in the SAED pattern (see white arrows in Fig. 4(b)). The presence of the cubic $BaTiO_3$ structure cannot be excluded, however the relative intensities of the peak doublet suggest that the tetragonal phase is by large the principal one; however, the lack of the statistics does not allow any quantitative evaluation. Finally, there is no evidence of the presence of TiO_2 in the SAED, due probably to the sampling problem; indeed, the high level of spatial resolution of TEM may make it difficult to detect phases present in such small quantity, see Table 1.

Temperature dependence of the dielectric constant and loss of all samples were measured at 10 kHz, and the data is given in Fig. 5. BT2 sample has the largest dielectric constant followed by BT1 and BT4. BT2 also showed the lowest dielectric loss. A broad peak in the dielectric constant can be observed for all samples at around 130 °C, marking the ferroelectric-paraelectric phase transition. All peak temperatures are included in Table 1. Differences in the transition temperatures of the samples might have been caused by the diffuse nature of the phase transition which was likely originate from the coexisting tetragonal and cubic phases. Such a diffuse phase transition was previously reported for cold sintered $BaTiO_3$ [16]. As the tetragonality increases, the dielectric peak at the Curie becomes sharper and transition becomes less diffuse with lower Curie temperature. BT2 had the highest tetragonality and showed the sharpest phase transition and in turn the lowest phase transition temperature of 135 °C quite similar to that of conventionally sintered $BaTiO_3$. In contrast, BT3 and BT4 with the lowest tetragonality values demonstrated the broadest phase transition with the largest transition temperatures. In addition to tetragonality, the amount of residual phases also affect the dielectric properties. BT2 sample which was subjected to hydrothermal process at 240 °C for 72 h, has the
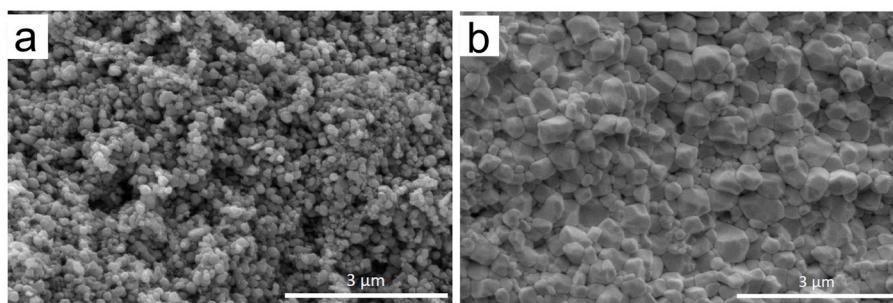

Fig. 3. SEM images taken from the fracture surfaces of **(a)** green-body, **(b)** BT2 sample obtained by hydrothermal reaction at 240 °C for 72 h.
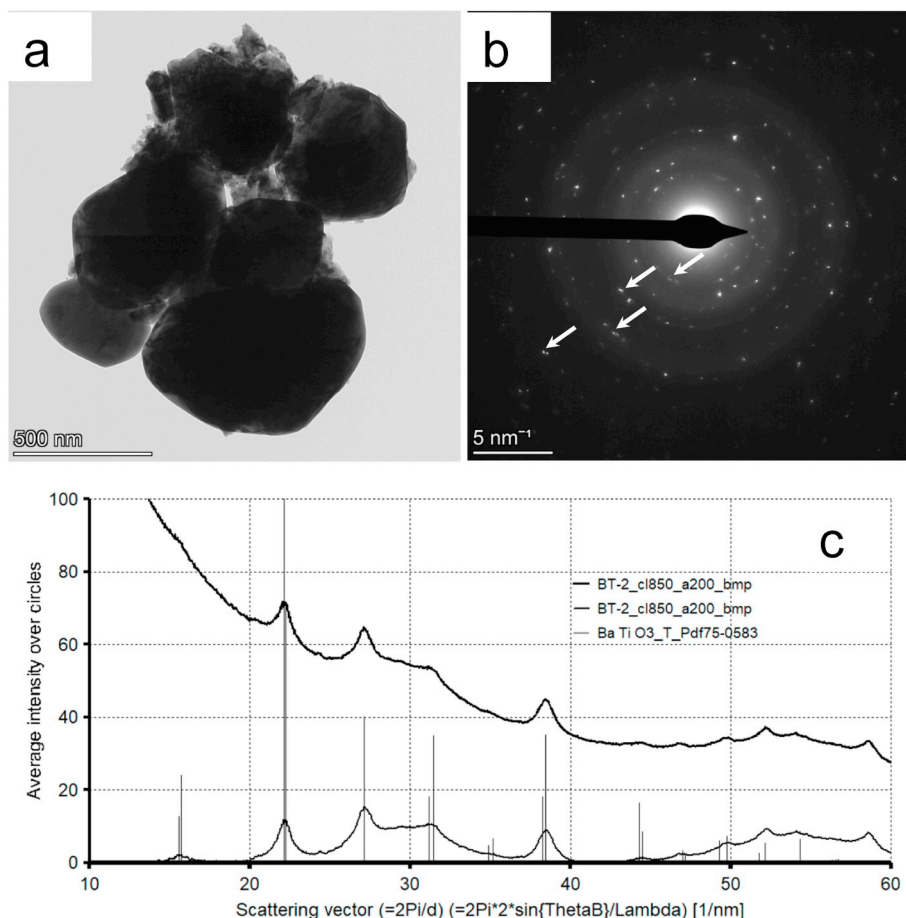
Fig. 4. TEM analysis of BT2 sample obtained by hydrothermal reaction at 240 °C for 72 h **(a)** image of an agglomerate, **(b)** SAED of the agglomerate, **(c)** integration of the SAED and its comparison with $BaTiO_3$ tetragonal card.
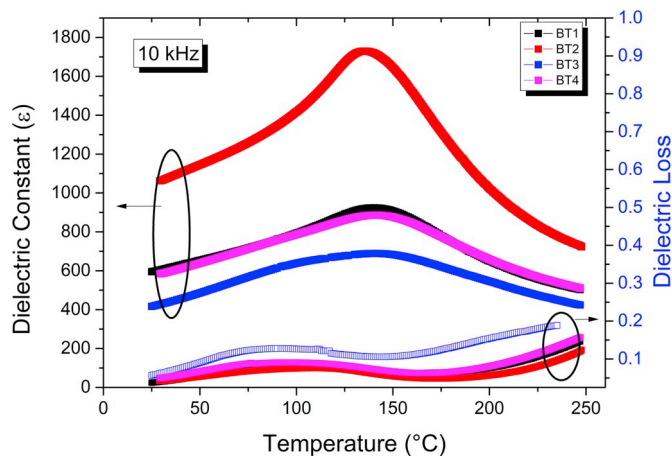

Fig. 5. The temperature dependence of the dielectric constant, and dielectric loss at 10 kHz.

highest amount of $BaTiO_3$, tetragonality as well as the lowest amount of residual titania; all of which accounts for the best dielectric properties i.e. sharpest phase transition and largest dielectric peak at the transition. This is in agreement with previous study on cold-sintering of $BaTiO_3$, where the dielectric peak at the phase transition could only be obtained after the additional heat treatment at 700 °C, which did not increase the relative density much (relative density was already 93% after cold sintering at 180 °C) but increased the tetragonality significantly [16].

Similar dielectric behavior, i.e. broad peak at the Curie temperature and relatively low dielectric constant was very recently reported for cold sintered $BaTiO_3$ ceramics obtained at 300 °C and explained mainly in terms of grain size effects [32]. Together with this recent report, the data in the current work supports that it is possible to obtain decent dielectric properties even by sintering at low processing temperatures via rHLPD.

In Fig. 6(a-d), ferroelectric hysteresis loops measured at 1 Hz and under different voltages are given. The applied electric field was increased gradually until the samples experienced dielectric breakdown. Hysteresis loops for all samples reached saturation before the dielectric breakdown took place. In Fig. 6(e), hysteresis loops for all samples measured up to 50 kV/cm are provided for comparison. BT2 had the largest saturation polarization followed by BT1, BT4 and BT3. This order was the same as for the dielectric constant and should also be related with the purity of the sample as well as its tetragonality level. The largest saturation polarization values obtained in this study on BT2 sample were lower (less than half) than that of the recently reported ones [32]. This difference might be related to few factors including the residual titania in the samples, and the dissimilarities in the processing temperatures (60° lower reaction temperature was used in the current study) which resulted in different densification levels and tetragonality. Coercive field (E_c) as well as remanent (P_r) and maximum polarization (P_m) values are also given in Table 1. BT2 having the lowest amount of residual impurities showed the smallest E_c whereas BT3 with the highest impurity content had the largest E_c. Impurity phases are known to impede domain wall motion and thus increase the coercive field [33].

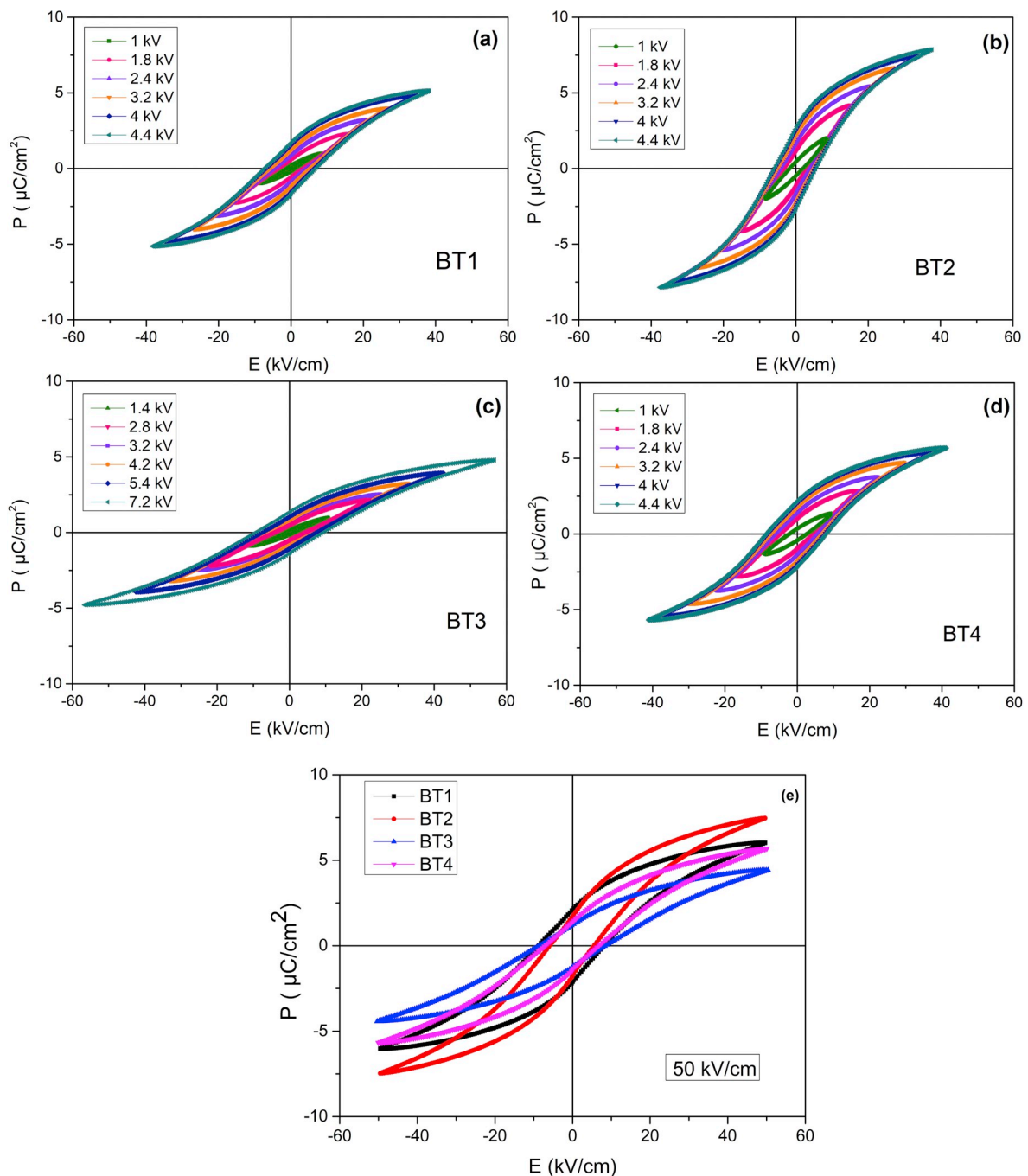To complement the ferroelectric hysteresis measurements,

Fig. 6. Development of ferroelectric hysteresis loops under increasing voltage **(a)** BT1, **(b)** BT2, **(c)** BT3, and **(d)** BT4, and **(e)** comparison of the hysteresis loops of all samples at 50 kV/cm.

displacement of the samples was measured and resulting strain values are shown in Fig. 7(a-d), together with the hysteresis loops obtained in the simultaneous measurement. For all samples, butterfly shaped strain loops are observed; slightly reaching negative values, indicating normal ferroelectric behavior [34]. Maximum strain of 0.05% at around 50 kV/cm was obtained again for the BT2 sample at around 50 kV/cm, consistent with its relatively large ferroelectric polarization and dielectric constant among other samples in this study.

Piezoelectric d_{33} coefficients (pC/N) of the samples were found to be 50 pC/N (for BT1), 84 pC/N (for BT2), 34 pC/N (for BT3), and finally 38 pC/N (for BT4). It should be noted that the poling process conditions (temperature and time) can be optimized to enhance the d_{33} values. Nevertheless, obtained values are much lower than that of the

conventionally sintered $BaTiO_3$ ceramics for which d_{33} values lie in the range of 350–500 pC/N [35]. Conventional sintering is typically done around 1350 °C and the resulting samples have relative density values greater than 95% [36].

4. Conclusions

$BaTiO_3$ ceramics were prepared via reactive hydrothermal liquid-phase densification (rHLPD) technique. The increase of both reaction time and temperature resulted in $BaTiO_3$ components having enhanced densification reaching to 86.8%. The samples showed acceptable electrical properties without any additional annealing processes. $BaTiO_3$ sample subjected to hydrothermal reaction at 240 °C for 72 h showed a
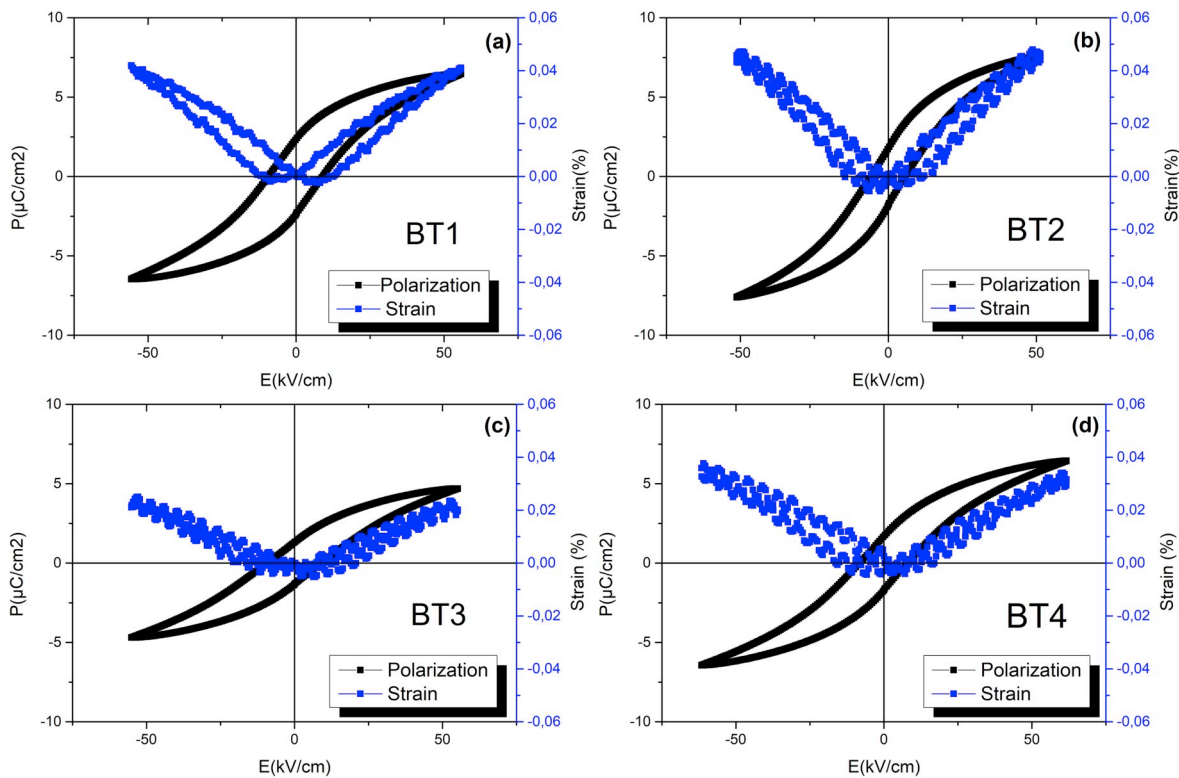
Fig. 7. Hysteresis (P–E) and Strain loops (S–E) of **(a)** BT1, **(b)** BT2, **(c)** BT3 and, **(d)** BT4 measured at 1 kHz.

saturated hysteresis loop and the corresponding butterfly shaped strain-electric field loop, together with a broad Curie temperature around 135 °C. The sample with the most favorable processing conditions yielded a piezoelectric coefficient d_{33} of 84 pC/N.

Declaration of competing interests

The authors declare that they have no known competing financial interests or personal relationships that could have appeared to influence the work reported in this paper.

Acknowledgments

References

[1] C. Vakifahmetoglu, L. Karacasulu, Cold sintering of ceramics and glasses: a review, Curr. Opin. Solid State Mater. Sci. 24 (2020) 100807, https://doi.org/10.1016/j.cossms.2020.100807.

[2] C. Vakifahmetoglu, Zeolite decorated highly porous acicular calcium silicate ceramics, Ceram. Int. 40 (2014) 11925–11932, https://doi.org/10.1016/j.ceramint.2014.04.028.

[3] C. Vakifahmetoglu, J.F. Anger, V. Atakan, S. Quinn, S. Gupta, Q. Li, L. Tang, R.E. Riman, Reactive hydrothermal liquid-phase densification (rHLPD) of ceramics–a study of the BaTiO₃ [TiO₂] composite system, J. Am. Ceram. Soc. 99 (2016) 3893–3901, https://doi.org/10.1111/jace.14468.

[4] X. Deng, X. Wang, H. Wen, A. Kang, Z. Gui, L. Li, Phase transitions in nanocrystalline barium titanate ceramics prepared by spark plasma sintering, J. Am. Ceram. Soc. 89 (2006) 1059–1064, https://doi.org/10.1111/j.1551-2916.2005.00836.x.

[5] G.H. Haertling, Ferroelectric ceramics: history and technology, J. Am. Ceram. Soc. 82 (1999) 797–818, https://doi.org/10.1111/j.1151-2916.1999.tb01840.x.

[6] T. Karaki, K. Yan, M. Adachi, Barium titanate piezoelectric ceramics manufactured by two-step sintering, Jpn. J. Appl. Phys. 46 (2007) 7035, https://doi.org/10.1143/JJAP.46.7035.

[7] X.H. Wang, X.Y. Deng, H.L. Bai, H. Zhou, W.G. Qu, L.T. Li, I.W. Chen, Two-step sintering of ceramics with constant grain-size, II: BaTiO₃ and Ni–Cu–Zn ferrite, J. Am. Ceram. Soc. 89 (2006) 438–443, https://doi.org/10.1111/j.1551-2916.2005.00728.x.

[8] H. Maiwa, Dielectric and electromechanical properties of BaTiO₃ ceramics prepared by hot isostatic pressing, Ferroelectrics 463 (2014) 15–24, https://doi.org/10.1080/00150193.2014.891419.

[9] H. Maiwa, Piezoelectric properties of BaTiO₃ ceramics prepared by hot isostatic pressing, J. Ceram. Soc. Jpn. 121 (2013) 655–658, https://doi.org/10.2109/jcersj2.121.655.

[10] T. Takeuchi, E. Betourne, M. Tabuchi, H. Kageyama, Y. Kobayashi, A. Coats, F. Morrison, D. Sinclair, A. West, Dielectric properties of spark-plasma-sintered BaTiO₃, J. Mater. Sci. 34 (1999) 917–924, https://doi.org/10.1023/A:1004506905278.

[11] T. Takeuchi, M. Tabuchi, H. Kageyama, Y. Suyama, Preparation of dense BaTiO₃ ceramics with submicrometer grains by spark plasma sintering, J. Am. Ceram. Soc. 82 (1999) 939–943, https://doi.org/10.1111/j.1151-2916.1999.tb01857.x.

[12] H. Maiwa, Electromechanical properties of BaTiO₃ ceramics prepared by spark plasma sintering and other methods, Jpn. J. Appl. Phys. 48 (2009), https://doi.org/10.1143/JJAP.48.09KD04 09KD04.

[13] J.-C. M'Peko, J.S. Francis, R. Raj, Field-assisted sintering of undoped BaTiO₃: microstructure evolution and dielectric permittivity, J. Eur. Ceram. Soc. 34 (2014) 3655–3660, https://doi.org/10.1016/j.jeurceramsoc.2014.04.041.

[14] R. Shi, Y. Pu, W. Wang, Y. Shi, J. Li, X. Guo, M. Yang, Flash sintering of barium titanate, Ceram. Int. 45 (2019) 7085–7089, https://doi.org/10.1016/j.ceramint.2018.12.211.

[15] H. Guo, A. Baker, J. Guo, C.A. Randall, Cold sintering process: a novel technique for low-temperature ceramic processing of ferroelectrics, J. Am. Ceram. Soc. 99 (2016) 3489–3507, https://doi.org/10.1111/jace.14554.

[16] H. Guo, A. Baker, J. Guo, C.A. Randall, Hydrothermal-assisted cold sintering process: a new guidance for low-temperature ceramic sintering, ACS Appl. Mater. Interfaces 8 (2016) 20909–20915, https://doi.org/10.1021/acsami.6b07481.

[17] H. Guo, A. Baker, J. Guo, C.A. Randall, Protocol for ultralow-temperature ceramic sintering: an integration of nanotechnology and the cold sintering process, ACS Nano 10 (2016) 10606–10614, https://doi.org/10.1021/acsnano.6b03800.

[18] J.-P. Ma, X.-M. Chen, W.-Q. Ouyang, J. Wang, H. Li, J.-L. Fang, Microstructure, dielectric, and energy storage properties of BaTiO₃ ceramics prepared via cold sintering, Ceram. Int. 44 (2018) 4436–4441, https://doi.org/10.1016/j.ceramint.2017.12.044.

[19] M. Biesuz, G. Taveri, A.I. Duff, E. Olevsky, D. Zhu, C. Hu, S. Grasso, A theoretical analysis of cold sintering, Adv. Appl. Ceram. 119 (2020) 75–89, https://doi.org/10.1080/17436753.2019.1692173.

[20] S. Grasso, M. Biesuz, L. Zoli, G. Taveri, A.I. Duff, D. Ke, A. Jiang, M.J. Reece, A review of cold sintering processes, Adv. Appl. Ceram. (2020) 1–29, https://doi.org/10.1080/17436753.2019.1706825.

[21] J. Cheng, Y. Chen, J.-W. Wu, X.-R. Ji, S.-H. Wu, 3D printing of BaTiO₃ piezoelectric ceramics for a focused ultrasonic array, Sensors 19 (2019) 4078, https://doi.org/10.3390/s19194078.

[22] M. Bortolotti, L. Lutterotti, I. Lonardelli, ReX: a computer program for structural analysis using powder diffraction data, J. Appl. Crystallogr. 42 (2009) 538–539,

https://doi.org/10.1107/S0021889809008309.

[23] N. Yasuda, H. Murayama, Y. Fukuyama, J. Kim, S. Kimura, K. Toriumi, Y. Tanaka, Y. Moritomo, Y. Kuroiwa, K. Kato, H. Tanaka, M. Takata, X-ray diffractometry for the structure determination of a submicrometre single powder grain, J. Synchrotron Radiat. 16 (2009) 352–357, https://doi.org/10.1107/S090904950900675X.

[24] M. Rezaee, S.M.M. Khoie, K.H. Liu, The role of brookite in mechanical activation of anatase-to-rutile transformation of nanocrystalline TiO_2: an XRD and Raman spectroscopy investigation, CrystEngComm 13 (2011) 5055–5061, https://doi.org/10.1039/C1CE05185G.

[25] S.M. Antao, I. Hassan, The orthorhombic structure of $CaCO_3$, $SrCO_3$, $PbCO_3$ and $BaCO_3$: linear structural trends, Can. Mineral. 47 (2009) 1245–1255, https://doi.org/10.3749/canmin.47.5.1245.

[26] P. Paufler, R.A. Young (Eds.), The Rietveld Method. International Union of Crystallography, Oxford University Press, 1993, p. 298, , https://doi.org/10.1002/crat.2170300412 Crystal Research and Technology 30 (1995) 494-494. ISBN 0-19-855577-6.

[27] J.O. Eckert Jr., C.C. Hung-Houston, B.L. Gersten, M.M. Lencka, R.E. Riman, Kinetics and mechanisms of hydrothermal synthesis of barium titanate, J. Am. Ceram. Soc. 79 (1996) 2929–2939, https://doi.org/10.1111/j.1151-2916.1996.tb08728.x.

[28] A. Chien, J. Speck, F. Lange, A. Daykm, C. Levi, Low temperature/low pressure hydrothermal synthesis of barium titanate: powder and heteroepitaxial thin films, J. Mater. Res. 10 (1995) 1784–1789, https://doi.org/10.1557/JMR.1995.1784.

[29] T. Tsumura, K. Matsuoka, M. Toyoda, Formation and annealing of $BaTiO_3$ and $SrTiO_3$ nanoparticles in KOH solution, J. Mater. Sci. Technol. 26 (2010) 33–38,

[30] T. Kubo, M. Hogiri, H. Kagata, A. Nakahira, Synthesis of nano-sized $BaTiO_3$ powders by the rotary-hydrothermal process, J. Am. Ceram. Soc. 92 (2009) S172–S176, https://doi.org/10.1111/j.1551-2916.2008.02739.x.

[31] J.L. Lábár, Consistent indexing of a (set of) single crystal SAED pattern(s) with the ProcessDiffraction program, Ultramicroscopy 103 (2005) 237–249, https://doi.org/10.1016/j.ultramic.2004.12.004.

[32] K. Tsuji, A. Ndayishimiye, S. Lowum, R. Floyd, K. Wang, M. Wetherington, J.-P. Maria, C.A. Randall, Single step densification of high permittivity $BaTiO_3$ ceramics at 300 °C, J. Eur. Ceram. Soc. (2019), https://doi.org/10.1016/j.jeurceramsoc.2019.12.022.

[33] T.E. Luke, Impurity control of domain switching in ferroelectric bismuth titanate, J. Appl. Phys. 45 (1974) 1605–1610, https://doi.org/10.1063/1.1663463.

[34] S.-T. Zhang, A.B. Kounga, E. Aulbach, T. Granzow, W. Jo, H.-J. Kleebe, J. Rödel, Lead-free piezoceramics with giant strain in the system $Bi_{0.5}Na_{0.5}TiO_3$–$BaTiO_3$–$K_{0.5}Na_{0.5}NbO_3$. I. Structure and room temperature properties, J. Appl. Phys. 103 (2008), https://doi.org/10.1063/1.2838472 034107.

[35] M. Acosta, N. Novak, V. Rojas, S. Patel, R. Vaish, J. Koruza, G.A. RossettiJr, J. Rödel, $BaTiO_3$-based piezoelectrics: fundamentals, current status, and perspectives, Appl. Phys. Rev. 4 (2017), https://doi.org/10.1063/1.4990046 041305.

[36] T. Karaki, K. Yan, M. Adachi, Subgrain microstructure in high-performance $BaTiO_3$ piezoelectric ceramics, Appl. Phys. Express 1 (2008) 111402, , https://doi.org/10.1143/APEX.1.111402.